Design strategies of three mirror design with freeform surfaces

Louis Duveau, Guillaume Druart, Thierry L Épine, Emmanuel Hugot, Xavier Briottet

DESIGN STRATEGIES OF THREE MIRROR TELESCOPES WITH FREEFORM SURFACES

OECD CONFERENCE CENTER, PARIS, FRANCE / 28 – 30 JANUARY 2020

Louis Duveau[1], Guillaume Druart[1], Thierry Lépine[2], Emmanuel Hugot[3], and Xavier Briottet[1]

[1] *ONERA - Office National d'études et de recherches aérospatiales, France*

[2] *Univ Lyon, Laboratory Hubert Curien, CNRS UMR 5516 - Saint-Etienne (France)*

[3] *Aix-Marseille Univ, CNRS, CNES, LAM - Marseille (France)*

KEYWORDS: freeform, optical design, straylight, infrared imaging, multispectral imaging, telescope

ABSTRACT:

In this paper we address the challenges posed by the use of these surfaces in optical design optimization, specifically the minimization of the surface counting, in order to simplify the manufacturing, assembly and integration phases. We focus on three mirror designs for infrared applications using a microbolometer and work on the compactness with various configurations in the 3D space. We will discuss our results on designs compatible with nanosatellites.

1 INTRODUCTION

The Urban Heat Island (UHI) is a phenomenon that most people are aware of. In urban areas, the intense human activity and energy consumed in a small area and the use of materials with a low albedo and high volumetric heat capacity increases this effect. The energy used to cool down buildings only add up to the problem [1]. To measure those effects, both on-site and remote data collection of temperature can be achieved. The on-site data represent the temperature inside the city and in the countryside at the same time repeatedly, but the spatial sampling of the data is then really sparse. To overcome this limitation, it is possible to use remote data from satellites like the Landsat satellites [2]. Such satellites are placed in sun-synchronous orbits[1], with long revisit periods (16 days for Landsat mission satellites). Such low revisit does not allow UHI analysis and its prediction. To increase the revisit frequency up to a few measurements per day, which is necessary to sample the circadian cycle, the number of satellites must be increased dramatically. However, such satellites embark high performance but expensive payloads and a constellation of this type of satellites is not financially reasonable.

To keep a good spatial sampling combined with a high revisit frequency, the use of multiple satellites in a constellation is mandatory but at a low cost and at a low mass. Therefore cubesats, which are small satellites of only a few cubic decimeters, are getting more and more popular for such scientific missions [3]. Such satellites can be mass-produced for a reasonable price. However, it implies the manufacturing of ultra compact optical payloads, which is possible using freeform surfaces. We define a freeform surface as a non-rotationally symmetric surface which cannot be described as an off-axis part of a conicoid.

The use of freeform surfaces allows an increase in performance such as on the field of view, the F-number, and the suppression of obscuration on all-reflective systems [4, 5]. This allow compact and well corrected off axis reflective designs. Reflective designs have the advantage of being light, achromatic, and potentially low-cost due to cheaper materials involved. It could result in industrial production of compact panchromatic systems for various applications ranging from automotive sensors to imaging cubesat [6].

In this article, we study the design of the telescope of a freeform off axis optical payload for a 12U[2] cubesat designed to measure land surface temperature. A constellation of such satellites could give access of a new and very useful database for climate studies including the study of urban heat islands worldwide. The technical choices for the optical design are explained in the first part. The second section explains the principles of freeform optical design.

[1] orbit around the earth in which the satellite always passes over any given point of the surface of the planet at the same local mean solar time

[2] 1U is one standardized unit of $10x10x10cm^3$

2 SPECIFICATIONS AND TECHNICAL CHOICES

Here are the principal requirements for the optical payload:

1. The payload must provide images in the thermal infrared spectrum. The measurement must be done in several spectral band to correct atmospheric and emissivity effects in order to retrieve the Land Surface Temperature.

2. The spatial resolution must be between 50 to 100m and the swath between 50 to 100km.

3. The whole satellite must be a 12U cubesat in low earth orbit altitude.

In order to keep a low cost, compact and easy to manufacture solution, we will study a design with an uncooled microbolometer and an off-axis unobscured telescope [7]. The use of a fully reflective design allows to consider for multispectral imaging by using a spectral separation after the last mirror. Indeed mirrors allows for an achromatic solution, and for an athermic solution if the whole instrument is made in the same material. Moreover mirrors are lighter than lenses and infrared optical materials are expensive. To produce an image of the scene with such a satellite, using a pushbroom[3] technique is very useful to have a simple and compact instrument. As presented in [8] and in figure 1 a two mirror freeform telescope is sufficient for this kind of mono-dimensional field. Finally, the third section presents the result design and an analysis of it.

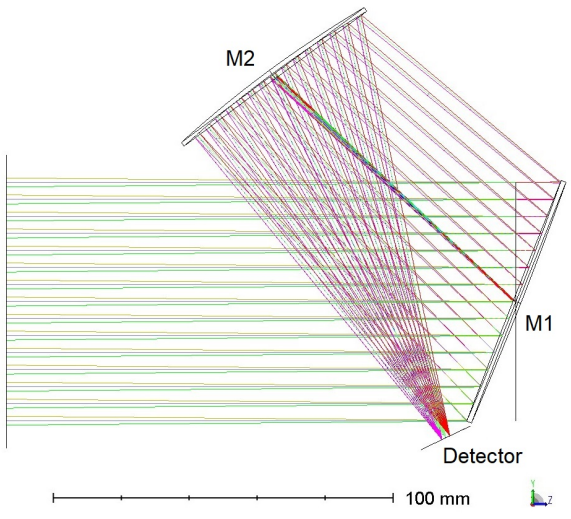

Figure 1: Example of a two mirror freeform telescope for pushbroom applications F#:2.1, f:150mm, fields: $1°Y$ $6°X$

However in this project, we need to have several spectral bands in the infrared (IR) spectrum. We also need to increase the time during wich a ground pixel is seen by the optical system, in order to increase the signal to noise ratio (SNR) by using post-processing Time Delay and Integration (TDI). To this end, we will increase the field of view of the system and use a full XGA matrix size of a microbolometer with a pixel pitch of 12μm. Such detectors are expected soon, as 12μm VGA and 17μm XGA detectors are already available. Using the whole detector will allow for the use of several filters and thus have a multispectral instrument in the thermal (or long-wave infrared - LWIR) spectrum (see figure 2). Using an off axis three mirror anastigmat (TMA) telescope for such a design is quite common [9, 10]. With an uncooled infrared detector, the system must have a low F number, under 1.5, to keep an acceptable NETD[4].

The spatial resolution is limited by the pixel size, which has an instantaneous field of view (IFOV) depending on the focal length of the instrument. Knowing the altitude, this IFOV can be expressed as dimensions of visible ground area, or ground sampling distance (GSD). The optical system modulation transfer function is also an important indicator to ensure that the Nyquist frequency of the detector is actually resolved. For this design we chose a 70m GSD, compliant with the requirements. The orbits have been calculated to be around 570km with a small eccentricity. The focal length can be deduced:

$$f = \frac{mean\,altitude * pixel\,size}{GSD} \approx 100mm \qquad (1)$$

But the image also suffer from motion blur due to the satellite movement above the ground. The mean orbital speed of this satellite would be:

$$v_0 = \sqrt{\frac{\mu}{a}} \approx 7,6km/s \qquad (2)$$

with μ the standard gravitational parameter and a the semimajor axis of the orbit.

This motion blur causes a loss in high frequency content and thus in resolution. To minimize the motion blur, the motion of the satellite in respect to the ground must be less than the GSD during the acquisition of an image. For a GSD of 70m and a displacement of 7600m/s, the ideal framerate would be 110Hz. In this paper, we anticipate that the technology will be available in a near future. However, the design presented can also be adapted for a bigger GSD with a higher aperture, trading spatial resolution for radiometric accuracy.

[3]The movement of the satellite above the scene allows to produce a two dimensional image with a mono-dimensional field of view of the optical system, orthogonal to the movement

[4]noise equivalent temperature difference

The half field of view (half FOV) along each direction is:

$$
\begin{aligned}
half\ FOV &= tan^{-1}(\frac{half\ image\ size}{f}) \\
half\ FOV\ X &\approx 3,5^\circ \\
half\ FOV\ Y &\approx 2,6^\circ
\end{aligned}
\tag{3}
$$

Finally, The whole 12U must be shared between the optical system, electronics and the platform subsystems, and we therefore decide to allocate only 8U to the telescope. Nevertheless, a standard 8U is a 20x20x20cm^3 cube which shape is not optimal for a TMA. Using a different subidivision of the satellite, we will choose an allocated volume of 130 x 250 x 200mm^3 (X,Y,Z) which is included in the 200 x 200 x 300mm^3 dimension of the satellite. Table 1 and figure 2 summarize the specifications of the optical payload.

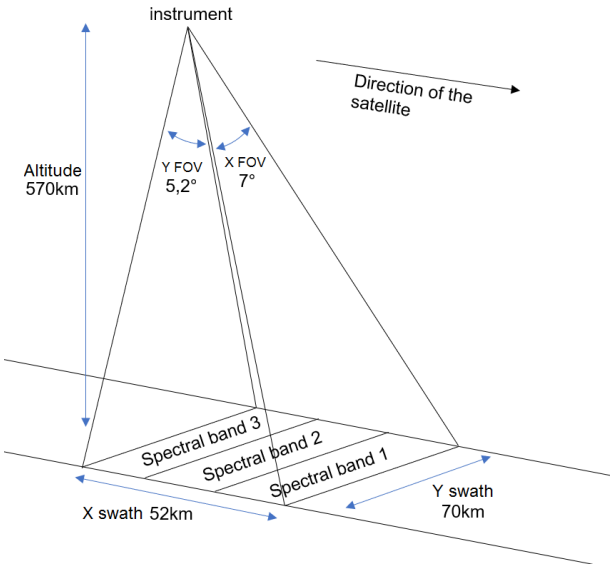

Figure 2: Summary of specifications and illustration of the field division for the multispectral imaging

Table 1: Summary of specifications

specification	value
effective focal length	100mm
half FOV X	3,5°
half FOV Y	2,6°
F#	1.5
pixel size	12μm
number of pixels	1024 X * 768 Y
max X dimension	130mm
max Y dimension	250mm
max Z dimension	200mm

3 FREEFORM OPTICS

Current optical systems are made of optical surfaces -mirrors or refractive surfaces- that are rotationnaly symmetric (as in figure 3) or decentered apertures of rotationnaly symmetric surfaces. This symmetry eases the design, manufacturing and test of such surfaces. But on axis reflective systems suffer from central obscuration that scales with the FOV. This central obscuration creates a modification of the diffraction pattern and a vignetting loss. To keep an unobscured design it is mandatory to decenter the surfaces, this decenter in increased if the system is designed for a large and potentially non symmetric FOV. But, such a decenter breaks the axial symmetry of the system. This asymmetry creates asymmetric aberrations that augment with the mirrors tilts and decenters, therefore being harder to compensate while keeping rotationnaly symmetric surfaces [11]. To remove those aberrations, non rotationnally symmetric surfaces can be used as in figure 4. These unconstrained surfaces, called freeform surfaces, can be designed to balance the off-axis aberrations.

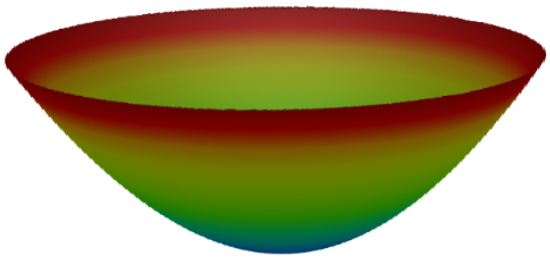

Figure 3: Spherical surface shape

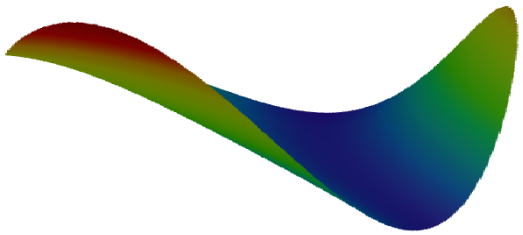

Figure 4: Example of a freeform shape

Freeform surfaces are mostly defined as a standard conic surface with a 2D polynomial correction, mostly over polar coordinates [5], but many other definitions exist, as Splines, Nurbs or radial basis functions[5] [12]. Reference [13] gives an overview of standard freeform surfaces description.

[5]Description of a surface with a base conic and multiple decentered radial basis functions, like gaussians

The two polynomial basis we will focus on are the Zernike polynomials and the XY polynomials:

$$Zernike : z(r,\varphi) = \frac{cr^2}{1+\sqrt{1-(1+k)c^2r^2}} + \sum_{i=1}^{N} A_i Z_i(\rho,\varphi) \tag{4}$$

$$XY : z(x,y) = \frac{cr^2}{1+\sqrt{1-(1+k)c^2r^2}} + \sum_{i=1}^{N} A_i E_i(x,y) \tag{5}$$

c is the curvature of the surface, k is the conic constant, Z_i is the ith Zernike polynomial, and E_i is the ith XY polynomial.

Every surface is then described by many coefficients instead of only 2 for a conic surface. This complexity is however overcame thanks to the high computational power of modern computers that can optimize on a large number of parameters, even if the optimization problem is a very complex issue that is studied by many researchers worldwide in numerous fields.

The most used definition is the normalized Zernike basis because it is an orthonormal basis over the unit disc. With a proper normalization, it is possible to have a unique description of the surface on the Zernike polynomial basis. Moreover, the Zernike polynomials are used to describe aberrations and it is often useful to look at the wavefront and the surfaces shapes with the same basis. However, in our design it was not efficient to use normalized Zernike polynomials. For our study, we performed an empirical try of both basis and the XY polynomials were more successful in optimizing a starting point with high off axis aberrations. However, performances could probably be increased with a proper normalization [14].

4 OPTICAL DESIGN AND ANALYSES

This optical system is designed with three freeform mirrors defined with XY polynomials. A standard optical design software have been used, while avoiding using any functions that use paraxial data. As an example, the design must ensure a symmetric resolution, thus keeping circular entrance and exit apertures. The focal length, being a paraxial value, is not relevant anymore. The focal length and distortion are kept by ensuring the same magnification as a 100mm classical design and this magnification is kept over the field by fixing the real image position and shape. The result is the TMA visible in the figure 5.

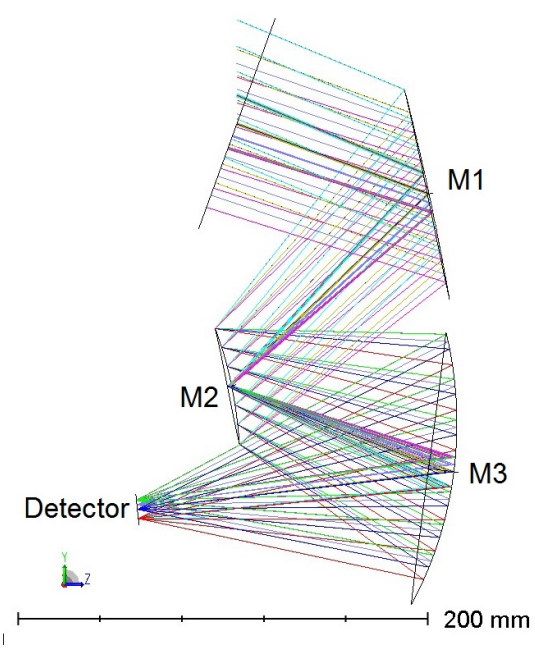

Figure 5: Layout of the optical system

The performances are visible in the figures 6 and 7. The optical system is diffraction limited for a 10μm wavelength and the total dimensions of the optical design is included in a 120*240*150mm (X,Y,Z) cube, leaving enough margin for mirror supports and detector integration.

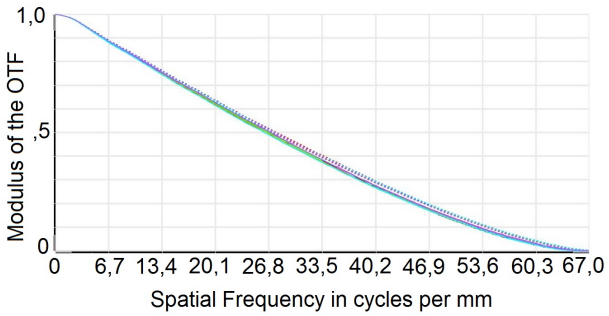

Figure 6: Modulation transfer function at 10μm. Detector Nyquist frequency: 42cy/mm

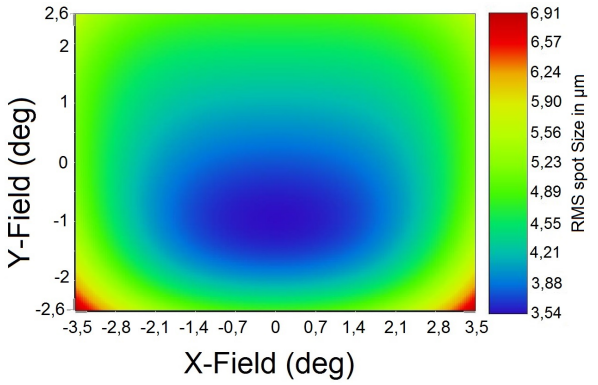

Figure 7: RMS spot radius over the field. Airy radius= 18,3μm Min RMS spot radius=3,5μm Max RMS spot radius=6,9μm

The accuracy of the temperature measurement is limited by the noise-equivalent temperature difference (NETD), the residual fixed pattern noise (RFPN) and the straylight.

This NETD is driven by the signal to noise ratio of the instrument. As uncooled microbolometers have a lower sensitivity than quantic detectors and a high thermal noise. To have a good sensitivity, the system should have a F-number as low as possible and working in wide spectral bandwidth.

The RFPN is also problematic. Microbolometers suffer from high fixed pattern noise which is usually corrected using a two-point correction. However, this spatial noise depends on the temperature of the detector, and the residual fixed pattern noise can limit the measurement accuracy. One possibility is to cool the detector (with a Peltier element as an example) but this solution implies higher costs and energy consumption and is less compact. A shutter migth be used for regular correction of this noise but it implies a moving part inside the system. Finally, the nominal solution is shutterless. A complete characterization of the instrument in a controlled environment is necessary to correct the fixed pattern noise for any detector temperature. The residual drift that may be caused by a lack of representativity of the lab calibration can be corrected with a cross calibration using data from another satellite over the same uniform scene (sea as an example), such as Meteosat satellites.

Finally, the last source of measurement error is the straylight variation. As the focal plane array is uncooled, so is the rest of the satellite. Every part located in front of the detector will emit infrared straylight and perturb the measurement. The straylight added by the system itself depends on its temperature, so this aspect must be measured to maintain both optical and radiometric performances. This measurement is performed during the characterization of the instrument mentioned above. This straylight is not critical as long as it stays stable (or predictable) over time. The out of field straylight is however more problematic. If such parasite light reaches the detector, it means that the unknown out of field temperature modifies the temperature measurement inside the FOV of the instrument. This implies that out of field straylight must be as limited as possible by design.

For this design, a specific set of constraints have been implemented to nullify the specular out of field straylight. Specular straylight is the straylight of an idealized system where mirrors have a reflection factor of one, and all the other parts absorb all light, without taking into account diffusion or emission by the surfaces. The constraints used are the following:

1. no ray must reach the detector without being reflected on the third mirror. This is reached by ensuring that the detector can only see the M3 or baffles.
2. no ray can reach the third mirror without being first reflected on the first and second mirrors or without having an high angle of incidence ensuring that it gets reflected on a surface far from the detector that can be hidden from it.
3. as any ray reaching the detector must be reflected by all three mirrors, by simple optical properties, it means that if it hits the detector it is a ray from inside the FOV of the instrument.

The first constraint is achieved using the secondary mirror as baffling, preventing rays from the first mirror to reach the detector, with an added baffle (blue in Figure 8) larger than the secondary to ensure this effect. In practice this baffle could be fixed on the secondary mirror support. As the detector is placed behind the secondary, no light can reach the detector from this mirror either. A second baffle (green) simulate the platform side (the distance between this baffle and the detector in the figure is not the maximum distance allowed by the allocated volume). Finally, a horizontal baffle (purple) prevent any ray going straight from the object space to the detector. The result is that the only optical element seen from the detector is the third mirror. The second constraint is achieved using the horizontal baffle: only rays that are far out of field can reach the third mirror. These rays with a high angle of incidence on the third mirror are reflected far from the detector, in the bottom of the satellite (they are represented in yellow in the figure 8). A baffling on the entrance aperture of the satellite (dark brown in the figure) could prevent most of these rays to reach the third mirror, limiting the amount of diffused light reaching the detector. The straylight analysis is summarized on the figure 8. The figure displays a non sequential ray tracing on the system, with the three added baffles. Four sources have been placed:

1. a collimated source at +2.6°Y for the red rays.
2. a collimated source at -2.6°Y for the green rays.
3. a lambertian source on the detector for the purple rays.
4. a quasi-lambertian source out of field for the yellow rays.

The green and red rays outlines the useful entrance beam, the yellow rays show the rays hitting directly the third mirror from the object space, and the purple rays are used to analyse potential straylight paths. If those rays are, after back propagation in the system, included in the red and green outlined beam in the object space it means that only useful rays from this beam can reach the detector.

Only the rays reaching the third mirror are drawn, as any ray that is not diffused or emmited inside the instrument is unable to reach the detector without first hitting this mirror thanks to the baffling. The green and red rays outlines the entrance beam and as pictured in the figure there are no ray emitted by the source on the detector that goes out of the field of view. By back propagation, this means that there are no out of field rays that can be reflected on the detector.

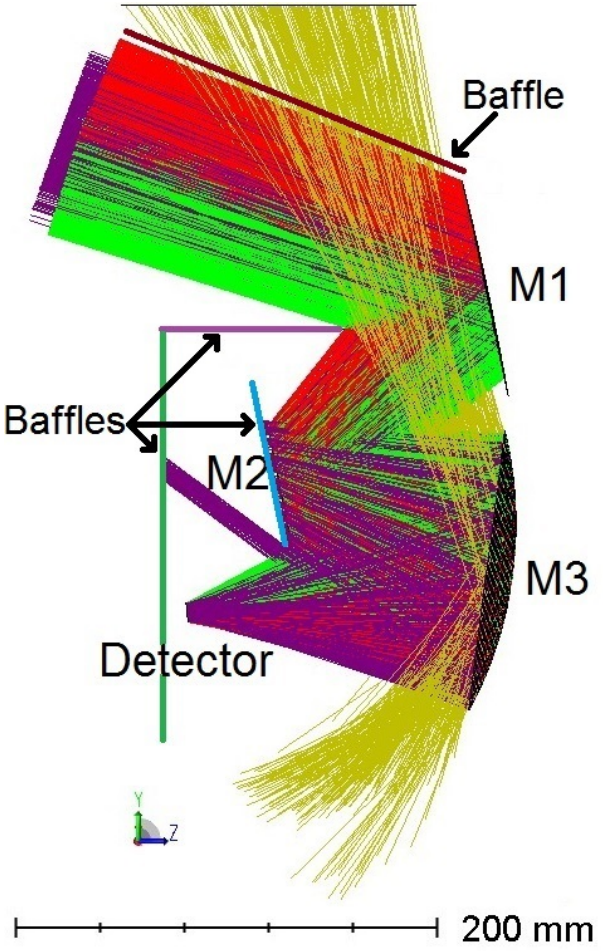

Figure 8: Straylight analysis summary of the optical system

The oblique purple rays are reflected on the bottom of the third mirror that would be cut out in the final design, as visible in the sequential ray tracing in figure 5. Even with a circulare mirror, these rays reach a baffle and thus there is no source in that direction.

This system is intended to be manufacturable. To assess the difficulty to manufacture the mirrors, the departures from the best spheres for each mirror are pictured on figures 9, 10 and 11.

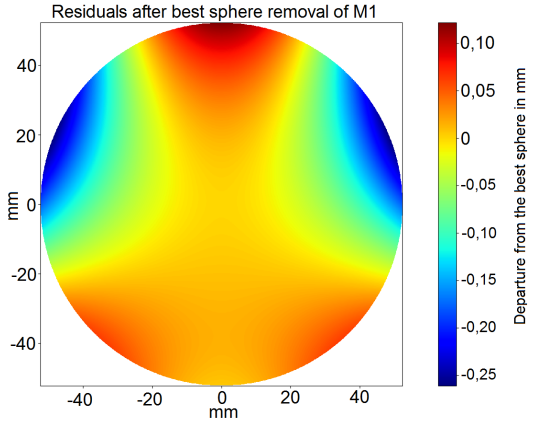

Figure 9: Residual sag of the M1 after removal of the best sphere fit. max departure: +/- 191μm

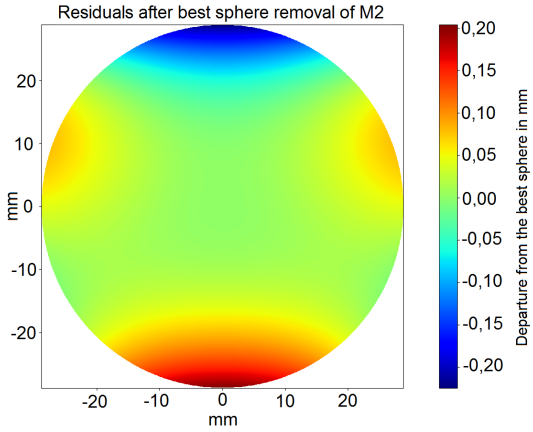

Figure 10: Residual sag of the M2 after removal of the best sphere fit. max departure: +/- 214μm

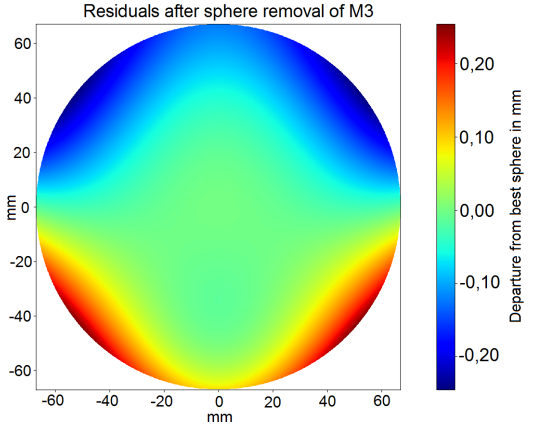

Figure 11: Residual sag of the M3 after removal of the best sphere fit. max departure: +/- 250μm

The results are to be taken with caution, as the mirrors have been calculated as circular while their real shape is different. It means that part of the residuals displayed will actually be on a part cut out of the final surface. A low departure from the best sphere and small local slopes would ensure that the surface could be tested with interferometry. However, there a many ways to perform metrology on freeform surfaces that are quickly improving [15].

As there are several techniques to manufacture freeform mirrors, the fabrication possibilities of freeform surfaces vary from one manufacturer to the other. For this reason, we plan to add manufacturer constraints directly in the merit function for further optimization of this design.

Finally, the length between the last mirror and the detector has been kept long enough to ensure that a dichroic filter can be placed to allow the use of a second detector, in the short wave infrared (SWIR) spectrum as an example. The principle is depicted in the following figure, where detector 1 is an uncooled microbolometer and the detector 2 is a SWIR detector:

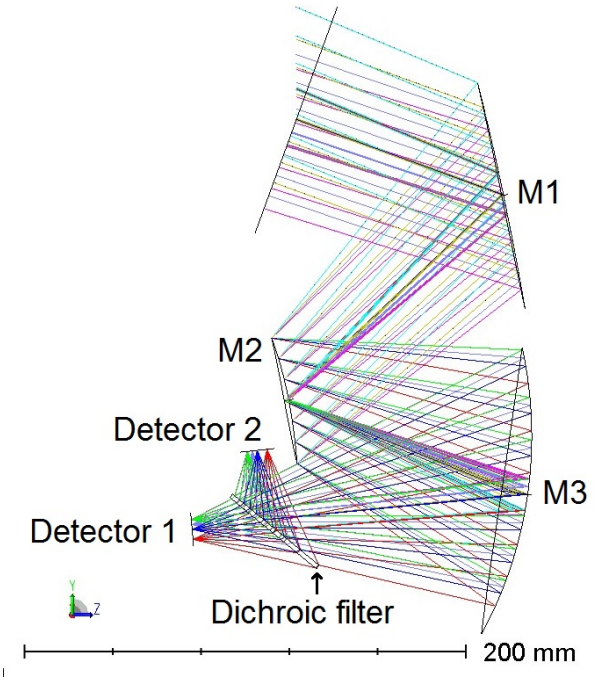

Figure 12: Layout of a multi spectral bands solution with a 2mm germanium dichroic filter

The mirrors are unchanged, so the performances for the reflected wavefront should also be identical. The performances for the transmitted wavefront are lowered due to aberrations added by the filter. Here we focus on the reflected wavefront, and the expected performances of the system for a 15μm pitch VGA SWIR detector (1 to 1.6μm). The image quality is very good.

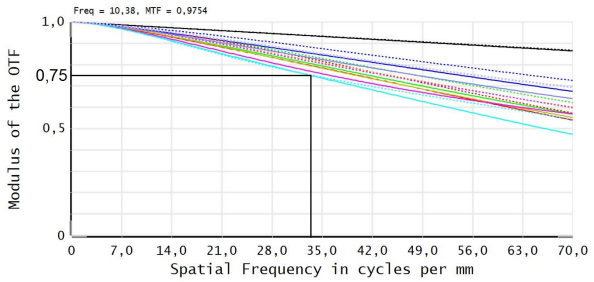

Figure 13: MTF for the SWIR (wavelength: 1μm). at Nyquist Frequency (33,3cy/mm) the MTF is above 70% between 1 to 1.6μm

5 CONCLUSION

In this article we presented a practical example of a freeform optical design for a nanosatellite, to have a compact and lightweight infrared or multi-spectral instrument to perform land temperature measurements to study the urban heat island effect. The design is based on a high aperture unobscured freeform TMA without specular straylight and an uncooled microbolometer. The design and tools used to optimize it have been kept versatile enough to ensure further optimization taking manufacturer capabilities into account or missions modifications as adapting the spectral bands of the instrument.

AKNOWLEDGMENT

This work was supported by the french agency for defense innovation: *Agence de l'Innovation de Défense (AID), France*.

REFERENCES

[1] M. Santamouris. "Regulating the damaged thermostat of the cities—Status, impacts and mitigation challenges". en. In: *Energy and Buildings* 91 (Mar. 2015). VIII4, pp. 43–56.

[2] Abbas Mohajerani, Jason Bakaric, and Tristan Jeffrey-Bailey. "The urban heat island effect, its causes, and mitigation, with reference to the thermal properties of asphalt concrete". en. In: *Journal of Environmental Management* 197 (July 2017). VIII1, pp. 522–538.

[3] Armen Poghosyan and Alessandro Golkar. "CubeSat evolution: Analyzing CubeSat capabilities for conducting science missions". en. In: *Progress in Aerospace Sciences* 88 (Jan. 2017). VIII2, pp. 59–83.

[4] Kevin P. Thompson and Jannick P. Rolland. "Freeform Optical Surfaces: A Revolution in Imaging Optical Design". en. In: *Optics and Photonics News* 23.6 (June 2012). I1, p. 30.

[5] Kyle Fuerschbach, Jannick P. Rolland, and Kevin P. Thompson. “A new family of optical systems employing phi-polynomial surfaces”. en. In: *Optics Express* 19.22 (Oct. 2011). II3, p. 21919.

[6] M. Esposito and A. Zuccaro Marchi. “In-orbit demonstration of the first hyperspectral imager for nanosatellites”. en. In: *International Conference on Space Optics — ICSO 2018*. Ed. by Nikos Karafolas, Zoran Sodnik, and Bruno Cugny. V6. Chania, Greece: SPIE, July 2019, p. 71.

[7] Guillaume Druart et al. “Study of infrared optical payloads to be integrated in a nanosat”. en. In: *Optical Design and Engineering VII*. Ed. by Laurent Mazuray, Rolf Wartmann, and Andrew P. Wood. V4. Frankfurt, Germany: SPIE, June 2018, p. 18.

[8] Jean-Baptiste Volatier, Louis Duveau, and Guillaume Druart. “An exploration of the freeform two-mirror off-axis solution space”. In: *Journal of Physics: Photonics* (in press 2019). III7.

[9] Thierry Lépine et al. “Advanced optical freeform substrates fabricated by ceramic 3D printing and controlled by deflectometry”. en. In: *Optical Fabrication, Testing, and Metrology VI*. Ed. by Sven Schröder and Roland Geyl. V3. Frankfurt, Germany: SPIE, June 2018, p. 24.

[10] Jun Zhu et al. “Design of a low F-number freeform off-axis three-mirror system with rectangular field-of-view”. en. In: *Journal of Optics* 17.1 (Jan. 2015). II22, p. 015605.

[11] Kevin P. Thompson et al. “Using nodal aberration theory to understand the aberrations of multiple unobscured three mirror anastigmatic (TMA) telescopes”. en. In: ed. by José Sasián and Richard N. Youngworth. II28. San Diego, CA, Aug. 2009, 74330B.

[12] Ozan Cakmakci et al. “Application of radial basis functions to shape description in a dual-element off-axis magnifier”. en. In: *Optics Letters* 33.11 (June 2008). II5, p. 1237.

[13] H. Gross et al. “Overview on surface representations for freeform surfaces”. en. In: ed. by Laurent Mazuray, Rolf Wartmann, and Andrew P. Wood. III6. Jena, Germany, Sept. 2015, 96260U.

[14] Eduard Muslimov et al. “Combining freeform optics and curved detectors for wide field imaging: a polynomial approach over squared aperture”. en. In: *Optics Express* 25.13 (June 2017), p. 14598.

[15] E. Savio, L. De Chiffre, and R. Schmitt. “Metrology of freeform shaped parts”. en. In: *CIRP Annals* 56.2 (2007). VII1, pp. 810–835.